3.2 AN EVALUATION OF FDS AND CLARK COUPLED WILDFIRE MODEL

Ruiyu Sun[1] * and Steven K. Krueger[1] and Mary Ann Jenkins[2] and William Mell[3] and Joseph J. Charney[4]
[1]University of Utah, Salt Lake City, Utah
[2]York University, Toronto, Canada
[3]National Institute of Stardards and Technology,Gaiithersburg,MD
[4]United States Forest Service, North Central Research Station,Easy Lansing,MI

1. Introduction

Wildland fire is a natural phenomenon involving complex chemical and physical processes. The range of length scales for each process is large, from the submillimeter scale (combustion process) to the kilometer scale (convection process). In the evolution of a large wildland fire, the interactions between the flame and the fire plume and the local close–in and larger–scale environment are important. The fires studied by Baum (2000) can be characterized by the nature of their interaction with the local environment, where the local environment is defined by the geometry and burning characteristics of the fuel bed, the properties of the ambient close–in atmosphere, and the local topography. The two most important interactions therefore are between the fire flame and the fuel (hereafter referred to as flame–fuel interaction), and between the fire flame and plume and the ambient atmosphere (hereafter referred to as flame+plume–atmosphere interaction). The flame–fuel interaction involves gas generation by solid fuel pyrolysis, the subsequent combustion of the fuel gases, and the resultant heat flux back to the solid fuel. The flame+plume–atmosphere interaction involves the response of the fire flame and plume to the ambient atmospheric conditions and the response of the atmosphere to the buoyant fire plume. This interaction can alter the orientation and geometry of the fire flame and plume, influencing the distribution and intensity of the net heat flux to the solid fuel and the burning of the fuel (Mell et al 2005), and consequently changing the properties of local atmospheric conditions.

It is extremely difficult to study wildland fires by direct observation. Along with the cost and safety issues, controlled fire experiments are practically impossible to achieve in a natural setting. For these reasons current computational fluid dynamical models are important tools for the study of wildfire, especially severe wildfire.

Because of the wide range of scales involved in a wildland fire, it is not possible to develop models that include all scales. Therefore, depending on the modeler's interests, each fire model concentrates on modeling wildfire behavior within a certain scale range. According to Mell et al (2005), there are four basic types of models depending on whether the two interactions are involved: operational models that do not explicitly include the two interactions; models that mainly involve the flame+plume/atmosphere interaction; models that mainly involve the flame/fuel interaction; and models that include both interactions to a greater or lesser degree.

The Clark coupled atmosphere–fire model (Clark et al 1996; hereafter referred to as the Clark coupled model) is an example of a wildfire model that emphasizes the interaction between the fire plume and the atmosphere, and is designed to simulate wildland fires over scales where a typical computational grid size of 10s of meters is too coarse to resolve physical processes in the combustion zone. Evolving model winds from the lowest levels of the atmospheric fluid dynamical model are passed to an operational empirically–based fire–spread–rate formulation (e.g., Hirsch 1996, Rothermel 1972) which is used to advance the fireline (Clark et al 2004). Because the thermal degradation of the solid fuel is not modeled directly and combustion is parameterized, computational resources are devoted to resolving atmospheric physics.

Examples of a wildfire modeling approach similar to the multiphase models that involve both interactions are the Fire Dynamic Simulator (FDS) and FIRETEC. FIRETEC was designed at the Los Alamos National Laboratory (Linn 1997; Linn et al 2002; Linn et al 2005) and built to analyze complex wildfire behavior that the current operational empirically–based wildfire models cannot represent. The FDS was designed at the Institute of Standards and Technology (NIST) and originally built to analyze industrial-scale fires. Mell et al (2005) has extended the FDS to simulate outdoor fires in vegetative fuels (called WFDS for Wildland Fire Dynamics Simulator). In these models the pyrolysis of fuels and gas phase combustion are implemented in a numerical solution of the Navier-Stokes equations, appropriate for low-speed, thermally-driven flow with

* *Corresponding author address:* Department of Meteorology, University of Utah, Salt Lake City, UT 84112. E-mail: rsun@met.utah.edu

an emphasis on smoke and heat transport from fires. Computational resources are devoted to resolving fire combustion and the close–in fire/atmosphere flow over the fire.

Though capable of accounting for almost all the variables that exist in wildfire prediction, the computational fluid dynamical models are not yet suitable for faster–than–real–time applications on today's computers. Such models can be used to improve our comprehension of wildfire and the accuracy of operational wildfire models to forecast actual fire spread and behavior. Before applying these wildfire simulation models to these problems, model validation is necessary. We need to compare model results to real fires.

Proper model evaluation requires an appropriate set of field observations, taken under well–documented and controlled conditions, and carefully analyzed for fire behavior. In the so–called "Meteotron" fire experiment, Benech (1976) presented the results of measurements in and around convective plumes initiated in the atmosphere from the ground by an exceptionally powerful artificial heat source. The experimental project was designed to provide data for theoretical study of a stationary, non-spreading, convective fire plume.

The purpose of this report therefore is to use the results from the Meteotron fire to examine how well the FDS and Clark model depict low–level structure/properties of this type of fire plume. A fire plume represents how the major portion of the energy from the fire's combustion process is put into the atmosphere and the resulting buoyancy distribution. The plume is one mechanism for the flame+plume–atmosphere interaction. The turbulent characteristics of the plume also mean that surrounding air will be entrained into the plume and consequently a flow will be induced in the air surrounding the fire. Once we demonstrate here how accurately the FDS and the Clark coupled model simulate the properties and behavior of a stationary, non-spreading plume, we can begin to use WFDS, a physically–based multiphase fire model, to improve the fire parameterizations for spreading fires utilized by wildfire coupled models and the forecast accuracy of operational models like FARSITE.

2. The Meteotron Experiment

From 1971 to 1973 Benech (1976) conducted eleven atmospheric fire plume experiments during the Meteotron fire experiment. The heat source consisted of 97 burners arranged into a hexagonal area of about 4000 m^2 (radius 36 m). The experiments generally lasted five to ten minutes, and in most of the experiments the total theoretical thermal power was about 600 MW. Measurements were taken using a radiosonde-radiowind system, kite balloons, photogrammetry from four observing stations, a ground network of temperature and wind velocity sensors, and an aircraft. The plume's geometrical parameters, including radius (accuracy estimated at 10%) and vertical velocity at the visible boundary of the plume, delimited by thick black smoke, were determined by a photogrammetric method (Saporte 1966). Temperature and vertical velocity measurements were made directly in the plume with a radiosonde system using a kite balloon. Below 600 m, plume–averaged vertical velocity data were obtained with photogrammetry and the radio-sounding kite balloon, while at higher altitudes these data were obtained only with photogrammetry of the rising plume edge.

Benech (1976) claimed that the following plume properties remained practically identical below the first 600 m of elevation for all experimental fires:

- plume averaged radius at a given altitude;
- plume vertical velocities at a given altitude;
- vertical flux ($m^3\ s^{-1}$) at a given altitude, deduced from the former data;
- and temperature difference (hereafter referred to as temperature excess) between the inside and the outside of the plume at a given altitude.

In the following sections, the FDS and Clark coupled model simulations are compared to the Meteotron mean plume radius, vertical velocity, mass flux, and temperature excess (temperature difference between the plume–averaged temperature and environment–averaged temperature) taken from Figures 5, 6, 7, and 8 in Benech (1976), and the mean plume buoyancy flux constructed with these data.

3. Numerical Experimental Set-up

A single FDS simulation and two Clark coupled model simulations were completed, and results from the simulations are compared to each other and to the observational data from the Meteotron fire experiment.

The version of FDS used in this study is described by Mell et al (2005). The FDS domain was 400 m (x) $\times$ 400 m (y) $\times$ 600 m (z) and covered by a grid mesh of 100 (x) $\times$ 100 (y) $\times$ 100 (z). The vertical grid was stretched and vertical grid size was about 3 m near ground level. The model atmosphere was isothermal, with an ambient temperature of 30.85°C. A uniform wind of 3 m s^{-1} and constant with height blew into the domain from the west (in the positive x direction). To match the size and total heat release rate of the

Meteotron fires (4000 m^2; 600 MW), a square fire of 63.25 m $\times$ 63.25 m was set. The heat release rate per unit area was 150 kW m^{-2} and the simulation lasted 700 seconds.

The version of the Clark coupled model used in this study is described by Clark et al (1996) and Clark et al (2004). The two simulations by the Clark coupled model, denoted as *Clarka* and *Clarkb*, were initiated in an environment of neutral stability with a surface temperature of 30.85°C and pressure of 100 kPa. The background wind was uniform at 3 m s^{-1} from the west and constant with height. The x and y horizontal grid interval was 25 m. The vertical grid was stretched and vertical grid size was about 10 m near the ground. Two domains were used in the simulations, an inner domain 1.2 km $\times$ 1.2 km in area nested in an outer domain 6.45 km $\times$ 6.45 km in area. Fire combustion was represented by a surface sensible heat flux, and an assumption was made that roughly 30% of the total heat released by the model fires was lost by radiation to the surroundings (Koseki and Mulholland 1991). Only the heat remaining after the loss of radiation is exchanged directly with the atmosphere. A sensible heat flux of 160 kW m^{-2} was assigned to six surface–level grids in the inner domain so that the total surface heat release rate came to 600 MW as in the Meteotron experiment. The six surface grids made the total burning area in the Clark coupled model 3750 m^2, which given the 25 m horizontal grid size was as close as possible to the total burning area of Meteotron fire (4000 m^2). Simulations lasted an hour.

Clark et al (1996) used a simple extinction approach to treat the fire-atmosphere heat exchange to avoid excessive local heating of the atmosphere when the entire sensible heat released from the fire was deposited in a column above the fire. In this early work it was not possible to test that this simple extinction–depth approach was realistic or even necessary. Therefore, in this study, the sensible heat flux of the fire was put into the Clark coupled model atmosphere in two different ways. In simulation *Clarka*, the surface sensible heat was vertically distributed in the atmosphere over an e-folding distance or extinction depth of 50 m. In simulation *Clarkb*, all the surface sensible heat was put into the first vertical layer in the inner domain.

4. Method of Analysis

Accurate calculations of plume–averaged properties are dependent on an accurate determination of the edge of the plume. Benech (1976) used "thick black smoke" and a photogrammetric method (Saporte 1966), with an estimated accuracy of 10%, for plume edge determination in the Meteotron experiment. Using the plume soot density provided by the FDS simulation, photos of smoke, as in Figure 1, were generated based on a version of Beer's law used by Smokeview, the software visualization tool for FDS (Forney and McGrattan 2005). These photos were overlaid on a cross-section of soot density along the centerline of the fire domain (y=0). A soot density of 0.5 mg m^{-3} was selected to delineate the plume edge and effective radius. Locations with soot density greater than 0.5 mg m^{-3} were considered to be inside in the plume. This choice of plume edge criterion (referred to as soot plume hereafter) was supported by radial profiles of soot density at different height levels. Figure 2 shows how at 600 s into the FDS simulation soot density varies along the center line of the domain in the x direction and along the line through the point with the maximum soot density in the y direction. At lower levels (below 300 m), the area with soot density greater than 0.5 mg m^{-3} covered almost all the plume. For this reason, the results presented in this study focus on the lower portion of the fire plume.

The soot plume can not be used to determine plume properties in the Clark coupled model simulations. The Clark (1996) coupled model does not simulate smoke and soot (as does the Clark 2003 version, which was not available for this study), and therefore no direct comparison can be made between fire plumes in the Clark coupled model simulations and the Meteotron experiment. However comparisons can be made between the FDS and Clark coupled model plumes when each model's plume–averaged properties depends on a consistent determination of the plume's edge. It was assumed that the radial profile of vertical velocity w in the plume has a normal distribution, and the portion of each plume with

$$w > \frac{w_{\max}}{\exp(c)}, \tag{1}$$

where $w_{\max}$ is the plume's maximum vertical velocity, was selected for plume property calculations and comparisons between the simulations. Hereafter this method is referred to as the W plume. Based on Yih (1951), the constant c is given the value 1.38 in Equation 1.

Computational resources were limited for this study. As a result the horizontal domain sizes were not large enough to contain model simulations, and the fire plumes went out of the lateral boundary on the downwind side of the domain before they reached domain top. The plume started to go out of bounds at approximately 300 m AGL in the FDS simulation (Figure 1) and at approximately 340 m AGL in the Clark coupled model simulations (not shown). Above these heights,

plume–averaged properties were calculated based on the portions of the plumes inside of the domains. Again, consequently, the results presented in this study focus on the lower portion of the fire plume, below the first 300 m of elevation.

5. Simulation Results

5.1. Comparing Meteotron and FDS Plume Properties

Figure 3 shows vertical profiles of the Meteotron, and soot–plume and W–plume FDS plume–averaged temperature excess, vertical velocity, effective radius, and mass flux. Each temperature excess profile is similar in shape, decreasing quickly with height near the surface. Plume–averaged vertical velocity $\overline{w}$ profiles are also similar in shape. At lower levels the W–plume tends to have a bigger plume–averaged temperature excess and vertical velocity, and smaller plume–averaged radius than either the soot–plume FDS or Meteotron plume. The differences between profiles are due primarily to the soot plume including areas of negative and small values of w, while the W plume does not. Although not apparent from these profiles, but easily deduced from Figure 1, the FDS results show large fluctuations in $\overline{w}$ at these levels due to turbulent motion (shedding of large eddies by the convection); strong updrafts coexisted with weak updrafts, sometimes even downdrafts in the plume, which contributed to the smaller soot–plume averaged FDS $\overline{w}$. Effective radii in the simulated plumes were determined by calculating plume area in the horizontal and assuming that the plume edge is perfect circle. Figure 3 shows that the effective plume radius determined by the soot plume in the FDS is considerably smaller than the plume radius determined by a photogrammetric method in the Meteotron experiment. Again, the results presented in this study focus on the lower portion of the fire plume.

Figure 3 also shows the vertical profiles of plume mass flux calculated using

$$F_M = \overline{w}\pi R^2, \tag{2}$$

where $\mathbf{F}_M$ is the plume mass flux according to classical idealized plume theory, and $\overline{w}$ and R the plume–averaged vertical velocity and effective radius, respectively. There is agreement only near the surface; above the surface the total plume mass flux in FDS is only about half as large as the Meteotron F_M. The differences between Meteotron and the FDS plume mass flux are due mainly to the square dependence of mass flux on R.

An explanation for the discrepancies between plume–averaged properties is seen in Figure 4 which shows x-y cross-sections of the FDS soot–plume at 103 m and 201 m AGL near the end of the simulation (680 s, randomly picked). The outermost soot contour is 0.5 mg m^{-3}, corresponding to the edge of the plume. The shape of the plume is highly irregular, as in Figure 1, and Figure 4 shows that if the plume is viewed from a different angle, the difference in radius can be as large as $1/3$ the effective radius. Figure 5a shows how different plume–averaged effective radii are possible. Figure 5b shows that when the average value of the x direction and y direction bounded radii shown in Figure 5a and the averaged vertical velocity in the soot plume are used in the mass flux calculation, the FDS mass flux is closer to the Meteotron result than calculations based on the plume edge as a perfect circle. Note that the Meteotron plume radius, determined by photogrammetry, is only an estimate of the actual plume radius, and that vertical flux at a given altitude was deduced from former Meteotron data. Good agreement between Meteotron and simulated FDS plume properties can be achieved therefore depending on the method of analysis.

5.2. Comparing FDS and Clark coupled model plume properties

In an endeavor to make congruous comparisons between the plume properties in the two different model simulations, data in the FDS simulation were averaged horizontally and vertically to 24 m and near-ground 10 m grid sizes — as close as possible to the 25 m horizontal and 10 m vertical grid sizes in the Clark coupled model simulations — before calculating the plume properties based on the W plume. Horizontally averaged FDS grid values will hereafter be refereed to as a grid–area average, and horizontally and vertically averaged FDS grid values as a grid–volume average. Unless stated otherwise, all following comparisons between FDS and *Clarka* and *Clarkb* are based on grid–volume averaged FDS results.

Figure 6 shows the differences in the plume properties between before and after FDS averaging. Differences are most significant in the plume–averaged temperature excess and vertical velocity at levels below 300 m, where magnitudes were most reduced by this averaging. A comparison between Figures 6 and 3 shows that averaging of FDS data produced, incidentally, upper-level plume properties of larger magnitude than the Meteotron results.

Figure 7 shows W-plume vertical profiles of the plume–averaged temperature excess, $\overline{w}$, R, and plume mass flux F_M for the FDS and the Clark coupled model

simulations. Compared to FDS, the coarser horizontal and vertical resolutions in the Clark simulations resulted in significantly smaller plume temperature excesses and vertical velocities, especially below the first $\sim$ 50 m of elevation, and especially for *Clarka*. In *Clarkb* sensible heat from the fire was put into the lowest vertical layer in the model, and convection resolved by the Clark model took over to distribute and transport the energy. In *Clarka*, the same amount of the energy was distributed vertically, over more than one layer, resulting in a smaller and unrealistic temperature excess near the ground. Above 50 m AGL (Above groud level) the plume–averaged temperature excesses in *Clarka* and *Clarkb* become essentially equal.

Figure 7b shows the vertical profiles of $\overline{w}$. Although all three profiles are similar in shape, both Clark coupled simulations show significantly smaller $\overline{w}$ values compared to $\overline{w}$ in the FDS simulation. Since $\overline{w}$ in a convectively–driven plume is dominated by vertically integrated buoyancy, which is determined by plume temperature excesses, these differences in profiles are due to the fact that, in the lower portion of the plume, there was immediately more buoyancy in the FDS plume grid-scale volume averages compared to *Clarkb*, and then compared again to *Clarka*.

Figure 7c shows that the W–plume Rs in *Clarka* and *Clarkb* are significantly larger than the corresponding Rs in the FDS simulation. Larger grid size has a non–negligible impact on the W plume and its determination of R. Consequently the plume–averaged mass fluxes in *Clarka* and *Clarkb*, seen in Figure 7d, are also significantly larger than those in the FDS simulation, and coincidentally more comparable in magnitude and behavior to the Meteotron soot–plume radius and mass flux shown in Figure 3.

5.3. Comparing Meteotron and Simulated Buoyancy Fluxes

The buoyancy flux for the FDS simulation and the Clark coupled model simulations were analyzed, first within the confines of classical plume theory, and then using a more fundamental approach based on conservation of energy and mass, where by combining the conservation of mass and energy model equations, an expression for conservation of buoyancy flux is produced.

According to classical plume theory, convective buoyancy flux F_B is determined by

$$F_B = \overline{w}\,\overline{B}\,\pi R^2 \tag{3}$$

where $\overline{w}$, $\overline{B}$, and R are, respectively, the plume–averaged vertical velocity, buoyancy, and effective radius. Using this equation for F_B, Figure 8 shows the vertical profiles of the convective buoyancy flux for the Meteotron experiment and for the W–plume fire simulations. With the exception of *Clarkb* at $\sim$ 20 to 30 m elevation, the Meteotron F_B is considerably larger than the convective buoyancy flux from the simulations. Again, the Meteotron results reflect the entire plume radius, while the vertical profiles of convective buoyancy flux for the simulated plumes reflect the partial, W–plume, radius. Also the Meteotron buoyancy flux profile for F_B was deduced from plots of mean plume radius, vertical velocity, and temperature excess in Benech (1976), and not based on original observations. The Meteotron $\overline{B}$ assembled from these data is considered especially vulnerable to error at levels below 50 m, primarily due to the difficulty establishing an accurate temperature excess reading from Benech (1976). The spike in buoyancy flux near the ground in *Clarkb* is a result of depositing the entire sensible heat released from the fire into the first model layer above the fire. The FDS convective buoyancy flux profile lies between the *Clarka* and *Clarkb* profiles.

Conservation of buoyancy in the FDS simulation is determined by

$$\begin{aligned}\int_V \frac{\partial B}{\partial t}\,dV \;&+\; \int_{\partial V} B\,\vec{\mathbf{v}}_H\cdot\hat{\mathbf{n}}\,dS + \int_{bottom}^{top} B\,w\,dS = \\ &-\; \int_{\partial V} \vec{\mathbf{F}}\cdot\hat{\mathbf{n}}\,dS,\end{aligned} \tag{4}$$

where all variables in Equation 4 are defined in the Nomenclature. The terms on the left-hand side of Equation 4 are, respectively, buoyancy storage, buoyancy change due to the horizontal advection, and buoyancy change due to the convection in the layer. The term on the right-hand side is the buoyancy change due to SGS (sub-grid scale) process, radiation, and combustion. Given the boundary conditions, where $\vec{\mathbf{F}}$=0 at the top of the simulation domain, Equation 4 is used to calculate the FDS buoyancy flux $\vec{\mathbf{F}}$ at different height levels, where the total vertical buoyancy flux is the sum of the convective buoyancy flux and the vertical buoyancy flux due to the SGS process, radiation and combustion.

Conservation of buoyancy in the coupled Clark simulations is determined by

$$\begin{aligned}\int_V \frac{\partial B}{\partial t}\,dV \;&+\; \int_{\partial V} B\,\vec{\mathbf{v}}_H\cdot\hat{\mathbf{n}}\,dS + \int_{bottom}^{top} B\,w\,dS \\ &=\; \frac{g}{C_p\,\overline{\rho}\,\theta_e}\int_V \nabla\cdot(C_p\,\overline{\rho}\,K_H\,\nabla\theta)\,dV \\ &-\; \frac{g}{C_p\,\overline{\rho}\,\theta_e}\int_{\partial V} C_p\,\overline{\rho}\,\theta_e\,\vec{\mathbf{v}}\cdot\hat{\mathbf{n}}\,dS,\end{aligned} \tag{5}$$

where all variables in Equation 5 are defined in the Nomenclature. The difference between Equations 4

and 5 lies in the terms on the right-hand side of these equations. In Equation 5 these terms represent, respectively, the buoyancy change due to SGS heat flux and to the environmental heat flux. Because the Clark simulations were initiated in an environment of neutral stability, the environmental heat flux term in Equation 5 is zero. The total buoyancy change in the layer due to the resolved and unresolved vertical motion in the Clark coupled model simulations is therefore the sum of the vertical convection term, and the SGS heat flux term.

FDS profiles of the total vertical buoyancy flux, buoyancy flux by convection, and vertical buoyancy flux by SGS process, radiation and combustion, based on Equation 4, before and after grid–area averaging, are given, respectively, in Figures 9a and 9b. Total vertical buoyancy flux is essentially constant below 300 m, the height the FDS plume began to move out of the lateral domain boundary. Below $\sim$ 30 m, the convective buoyancy flux increases rapidly with height, while the SGS flux decreases rapidly with height. Above 30 m, convective buoyancy flux dominates to contribute to the total buoyancy flux, while SGS flux declines, quickly in Figure 9a and more gradually in Figure 9b, to near–zero values. Again, although not apparent from the profiles in Figure 9a, there are large fluctuations in FDS convective flux values due to turbulent motion. Consequently, Figures 9a and 9b show that the grid-scale convective buoyancy flux is made smaller and positive, while the sub-grid scale convective flux is made larger and all positive, by grid–area averaging.

Profiles of the total vertical buoyancy flux, buoyancy flux by convection, and the SGS heat flux based on Equation 5 for *Clarkb* and *Clarka* are given, respectively, in Figures 9c and 9d. The *Clarka* results (Figure 9d) are more similar to the after grid–area averaged FDS results (Figure 9b), while the *Clarkb* results (Figure 9c) are more similar to the before grid–area averaged FDS results (Figure 9a), in both behavior and magnitude. Note that there is little discernible difference between any of the profiles of the total vertical buoyancy flux in Figure 9.

The differences between Figures 9a and 9d are that *Clarkb* shows an even more abrupt increase with height in the convective buoyancy flux, and an even more abrupt decrease with height in the SGS flux in the first 30 m AGL. Above 30 m, the change with height stops and the convective buoyancy flux dominates to contribute almost entirely to the total buoyancy flux, while SGS flux falls to small near-zero (but all positive) values.

The differences between Figure 9b and 9c are that *Clarka* shows an even more gradual near-surface increase with height in the convective buoyancy flux, and an even more gradual decrease with height in the SGS flux, which eventually stop at $\sim$ 100 m AGL not $\sim$ 30 m AGL, compared to the *Clarkb* and the before grid–area averaged FDS profiles. Above 100 m, the *Clarka* SGS flux profile remains fairly significant and positive, making a relatively substantial contribution of the total buoyancy flux, while the contribution by the convective buoyancy flux is diminished compared to the FDS profile in Figure 9b.

Grid–scale buoyancy is a volume average of buoyancy of the combusting fluid and the atmosphere, while the fire–induced buoyancy is confined to the region containing combusting gases. Since FDS radiative and SGS scale energy transport calculations are more explicit and more realistically confined to regions containing combusting gases, it is assumed that the FDS profiles in Figure 9 describe reality best. By comparison, it appears that in *Clarkb* buoyancy is put into too shallow a surface layer by the SGS heat flux, and that in *Clarka* buoyancy is put into too deep a surface layer by the SGS heat flux.

6. Discussion

The FDS and the Clark coupled atmosphere–fire model, representing two types of fluid dynamical wildfire models, are used to simulate stationary, non-spreading fires in the Meteotron fire experiment and evaluated based on comparisons between Meteotron and simulated model fire plume properties. Agreement between Meteotron and simulated plume properties depended on both experiment and numerical model design, and the method of analysis of Meteotron and numerical model data. The numerical set-ups only approximated the environmental conditions during the Benech study. For example, in the FDS simulation the atmosphere was isothermal and in the Clark coupled model simulations the atmosphere was neutrally stable, while background winds in every simulation were constant in speed, direction, and height. An exact match to the Meteotron total burning area was not possible. Much of the analysis of the data and comparison of results depended on classical plume theory. Agreement between plume–averaged properties is constricted by a plume theory rendition, given its simplifying assumptions and idealized boundary conditions. Plume theory depends on plume–averaged properties based on accurate estimations of plume edge and an effective plume radius. Benech (1976) rated the accuracy of plume properties to be $\pm$10%. This study shows that the different methods for determining effective plume radius affect the analysis. However, despite these conditions, the study shows that agreement exists as evidenced by the comparison between the Meteotron and FDS soot–

plume properties, and then a comparison between the FDS and Clark coupled model W–plume properties.

Comparisons of the FDS plume–averaged properties to the Meteotron experiment indicate that, depending on the plume edge (soot or W) and the subsequent determination of effective radii and use of classical plume theory, the plume–averaged temperature excess and vertical velocity showed good agreement with the Meteotron experiment, while the plume–averaged effective radius and mass flux showed, depending on the method of analysis, good agreement. Comparisons of *Clarka* and *Clarkb* to the FDS W–plume averaged properties results indicate that the plume radius and mass flux in *Clarka* and *Clarkb* were similar,i and larger than FDS results. Near-surface temperature excess and vertical velocity were smaller in *Clarka* than in *Clarkb*, and both were smaller again than FDS results.

The Meteotron results and the FDS simulation demonstrate that the FDS can provide realistic plume–averaged properties. The comparisons between the FDS simulation and the Clark model simulations show that the coarser resolution of the coupled Clark model does reduce the accuracy of plume properties. Better agreement, especially in the first 10 to 30 m of elevation, between the Clark model and the Meteotron and FDS plume–averaged temperature excess and vertical velocity results was obtained when all the surface sensible heat was put into the first vertical layer (10 m elevation) of the coupled Clark model.

Using Meteotron as a benchmark, comparisons between the Meteotron and FDS, *Clarka*, and *Clarkb* buoyancy flux profiles indicate the following. Depending on the method of determination, the FDS and *Clarka* buoyancy flux showed similar overall behavior and magnitude, and fair to good agreement with the Meteotron experiment at elevations greater than 50 m AGL. As a result of depositing the entire sensible heat from the fire into the first 10 m AGL of the model atmosphere, *Clarkb* showed an abrupt spike in buoyancy flux near ground level, below the 50 m AGL, in partial agreement with the Meteotron experiment (shown) and before averaging FDS values (not shown).

Using FDS as a benchmark, the FDS, *Clarka*, and *Clarkb* conservation of buoyancy flux analysis indicates the following. The buoyancy flux by SGS motion and heating were more active close to the flaming zone of a fire, and directly influenced the vertical transport of energy only at near-surface elevations (which ranged from $\sim$ 30 to 100 m depending of the method of determination). At near-surface elevations, the convective buoyancy flux increased (very rapidly depending on the method of determination) with height, while the SGS flux decreased (very rapidly depending on the method of determination) with height to near–zero. At above near–surface elevations, the convective buoyancy flux made up almost the entire total vertical buoyancy flux, which was essentially constant with height.

Based on comparisons of the *Clarka* and *Clarkb* to the FDS and the Meteotron results, there is no clear, unambiguous choice of whether it is better to deposit the sensible heat released from the fire over a relatively large extinction depth of 50 m, as in *Clarka*, or over a first 10 m vertical layer as in *Clarkb*. The first method underestimates important near-surface properties just above the fire, such as temperature excess and vertical plume velocity, while the second method produces a too abrupt and discrete spike in convective buoyancy flux just above the surface model grid layer.

It seems likely then that a coupled model simulation would achieve more reasonable plume–averaged properties if a realistic extinction depth is adopted. Although the extinction depth depends on a number of parameters, such as fire intensity, flame height, burning fuel, the environment of the fire, etc., it is possible to estimate roughly what the extinction depth should be with

$$I/I_0 = e^{-KL}, \tag{6}$$

a form of Beer's law. Here I_0 and I are the radiation intensities at a wavelength before and after the extinction occurs, K is the extinction coefficient, and L is an attenuation length. Assuming that soot is the most important combustion product controlling the thermal radiation from the fire flame and hot smoke, then the extinction coefficient is $K = K_m \rho_s$, where K_m and ρ_s are the mass specific extinction coefficient and soot density. For flaming combustion of wood, K_m is 7600 m^2 kg^{-1} (McGrattan and Forney 2004). The averaged soot density below 100 m AGL was approximately 5 mg m^{-3} in the FDS simulation. Based on these assumptions, the approximated e–folding extinction depth is $\sim$ 25 m from the flame height, considerably less than the 50 m extinction depth used in part of this study.

7. Conclusions

According to classical plume theory (Morton et al 1956), one of the external parameters determining plume–averaged properties such as plume temperature excess and vertical plume velocity in a convective plume is the buoyancy flux at the source. If vertical velocity is known, then vertical mass flux is known, and vice versa. If vertical mass flux is known, then inflow velocity can be determined. Mass flux, vertical velocity, and inflow velocity are all related to plume height through atmospheric stability. Inflow velocity at the surface is connected to fire spread rate, which is connected to fire combustion and sensible

heat flux at the ground. These concepts based on classical plume theory contribute to our understanding of fire plume behavior. The study has demonstrated that the FDS, a physically–based multiphase fire model, is capable of rendering realistic plume–averaged temperature, vertical velocity, radius, mass flux, and buoyancy flux in a stationary, non-spreading convective fire plume. The study has also demonstrated that the Clark coupled model, designed to simulate wildland fires over scale lengths of atmospheric convection associated with large fire plumes and their environment, is likewise capable of rendering comparatively realistic plume–averaged properties, even when fire combustion is represented simply by a surface sensible heat flux, provided that the energy released from the fire is distributed vertically into a layer of ideal depth. Accurate sensible heating amounts and rates, and a stretched grid allowing for finer near-surface grid resolution, based on an energy extinction depth appropriate to the fire, are recommended to achieve realistic plume properties in a coupled model. This study serves as a guide towards our long-term goal to develop and test a simple, computationally efficient, and effective parameterization of fire combustion and wildfire spread that is "coupled" to the fire plume and the atmosphere. The next step is to extend the validation effort to a larger set of experiments (e.g., non–stationary, spreading fires) and to a wider range of fuel types and fuel parameters (e.g., moisture, surface to volume ratio, packing ratio) in order to better assess the WFDS capabilities. Once the WFDS is validated, we plan to use the WFDS to develop realistic parameterizations of fire spread and fire combustion for coupled atmosphere–wildfire model grid scales. A coupled wildfire model's ability to accurately predict local wind and the interaction of fire and wind makes it a major tool for studying severe fire behavior or large pyrocumulus development. As this study shows, coarser horizontal and vertical resolution results in averages over a larger grid-scale volume, and important plume properties that depend on smaller-scale fire/atmosphere interactions (i.e., temperature, vertical motions, vorticity) are under resolved. Numerical resolution is the important issue when developing and implementing a wildfire parameterization.

Nomenclature

A	horizontal grid area
B	acceleration due to buoyancy
B	$= g(T - T_e)/T_e$ in FDS
B	$= g(\theta - \theta_e)/\theta_e$ in Clark model
c	Yih (1951)'s constant
C_p	specific heat at constant pressure
$\mathbf{F}$	buoyancy flux due to sub-grid scale processes, radiation, and combustion
F_M	plume mass flux based on classical plume theory
F_B	convective buoyancy flux based on classical plume theory
F	buoyancy flux due to sub-grid scale processes, radiation, and combustion
g	acceleration due to gravity
$\widehat{\mathbf{k}}$	unit vertical vector
K_H	eddy mixing coefficient for heat and moisture
$\widehat{\mathbf{n}}$	unit normal vector
S	model level surface
t	time
T	absolute temperature
T_e	environmental T
$\mathbf{v}$	total wind velocity vector
$\mathbf{v}_h$	horizontal wind vector
V	model layer volume
w	vertical wind velocity component
$\overline{w}$	plume–averaged vertical wind velocity
ρ	total density of gas
$\overline{\rho}$	average density of gas over a model layer in simulation domain
θ	$= T(\frac{p_0}{p})^{R_d/C_p}$ potential temperature
θ_e	environmental potential temperature
∇	total gradient vector

References

[1] Baum, H. R., 2000: Modeling and scaling laws for large fires. In *Proceedings of ISSM-III Third International Symposium on Scale Modeling*, Nagoya, Japan, 1–13.

[2] Benech, B., 1976: Experimental study of an artificial convective plume initiated from the ground. *J. Appl. Meteor.*, **15**, 127–137.

[3] Clark, T., J. Coen, and D. Latham, 2004: Description of a coupled atmosphere-fire model. *International J. of Wildland Fire*, **13**, 49–63.

[4] Clark, T., M. A. Jenkins, J. Coen, and D. Packham, 1996: A coupled atmosphere-fire model: role of the convective froude number and dynamic fingering at

the fireline. *International J. of Wildland Fire*, **6**, 177–190.

[5] Finney, M. A., 1998: *FARSITE: Fire Area Simulator-Model, Development and Evaluation*. USDA Forest Service, Rocky Mountain Research Station.

[6] Forney, G., and K. McGrattan, 2004: User's guide for smokeview version 4; a tool for visualizating fire dynamics simulation data. Technical report, NIST. NIST Special Publication 1017.

[7] Hirsch, K. H., 1996: *Canadian Forest Fire Behavior Prediction (FBP) System: User's Guide, Special Report 7*. Canadian Forest Service, Northwest Region, Northern Forestry Center.

[8] Koseki, H., and G. W. Mulholland, 1991: The effect of fire diameter on the burning of crude oil pool fires. *Fire Technology*, **27**, 54–65.

[9] Larini M., F. Firoud, B. P., and J. C. Loraud, 1998: A multiphase formulation for fire propagation in heterogeneous combustible media. *Int. J. Heat Mass Transfer*, **41**, 881–897.

[10] Linn, R., 1997: *A transport model for prediction of wildland fire behavior*. PhD thesis, New Mexico State University.

[11] Linn, R., and P. Cunningham, 2005: Numerical simulations of grass fires using a coupled atmosphere-fire model: Basic fire behavior and dependence on wind speed. *J. Geophysical Research, to appear*.

[12] Linn, R., J. Reisner, J. J. Colman, and J. Winterkamp, 2002: Studying wildfire behavior using firetec. *International J. of Wildland Fire*, **11**, 233–246.

[13] McGrattan, K., 2004: Fire Dynamics Simulator (Version 4), Technical Reference Guide. Editor, McGrattan, K.B. NISTIR Special Publication, 1018, National Institute of Standards and Technology, Gaithersburg, Maryland. http://fire.nist.gov/bfrlpubs/.

[14] Mell, W., M. A. Jenkins, J. Gould, and P. Cheney, 2005: A physically based approach to modeling grassland fires. *International J. of Wildland Fire*, **To be submitted**.

[15] Morton, B. R., G. I. Taylor, and J. S. Turner, 1956: Turbulent gravitational convection from maintained and instantaneous source. *Proc. Roy. Sco. London*, **A234**, 1–23.

[16] Rothermel, R. C., 1972: A mathematical model for predicting fire spread in wildland fuels. In *Research paper INT 115, Intermountain Forest and Range Experiment Station Ogden, Utah, USA*.

[17] Saporte, R., 1966: Sur la determination de la hauteur d'un nuage d'apres deux vues photogrammetriques. *J. Rech. Atmos.*, **2**, 27–35.

[18] Yih, C. S., 1951: Free convection due to point source of heat. In *Proc. First U.S. Nat. Cong. App. Mech.*, p 941.

ACKNOWLEDGMENTS. This research was supported by the United States Department of Agriculture Forest Service Research Joint Venture Agreement 03-JV-11231300-08. A gratis grant of computer time from the Center for High Performance Computing, University of Utah, is gratefully acknowledged.

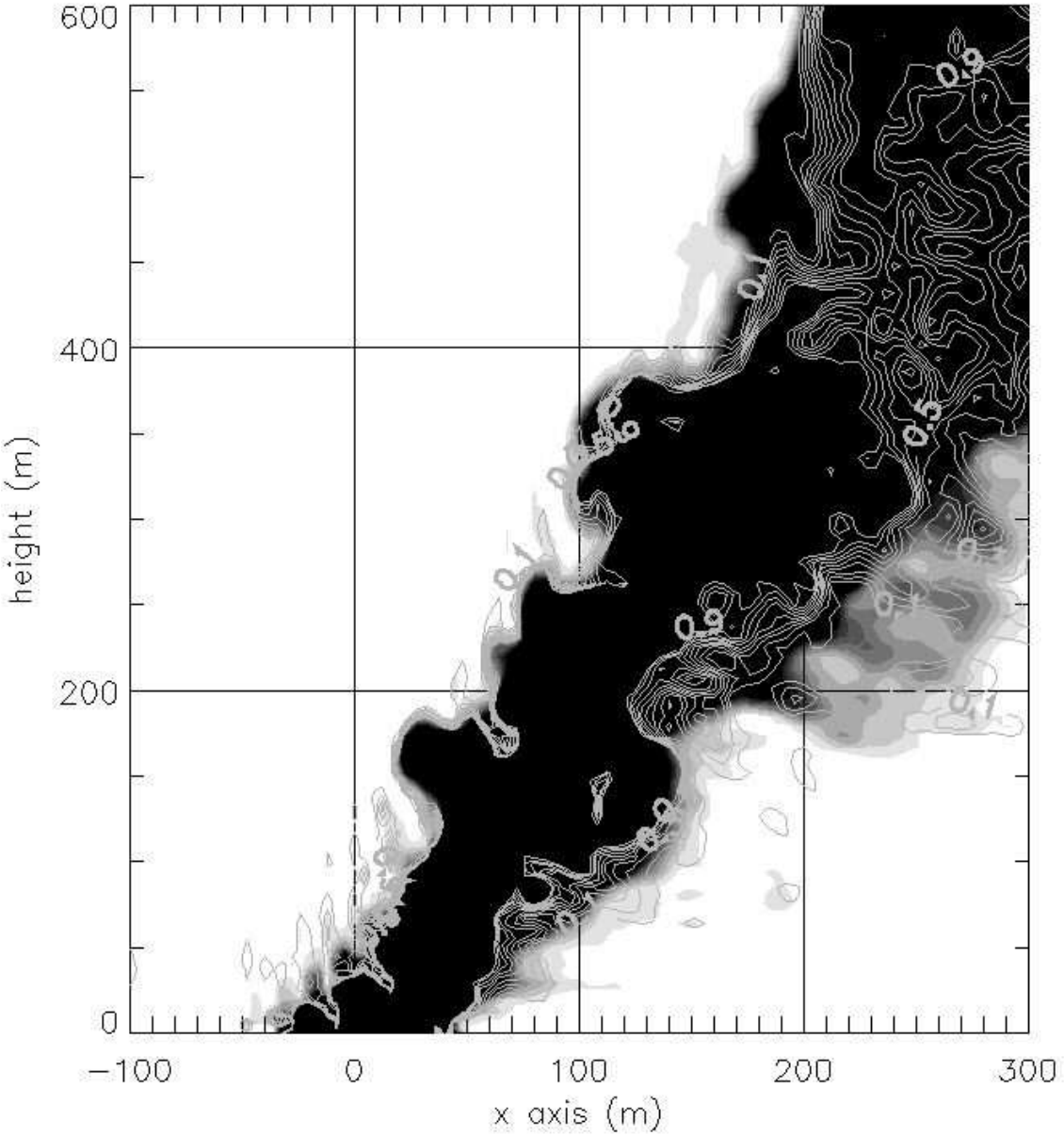

Figure 1: The x-z cross section of FDS smoke photo and soot density contours along the domain centerline.

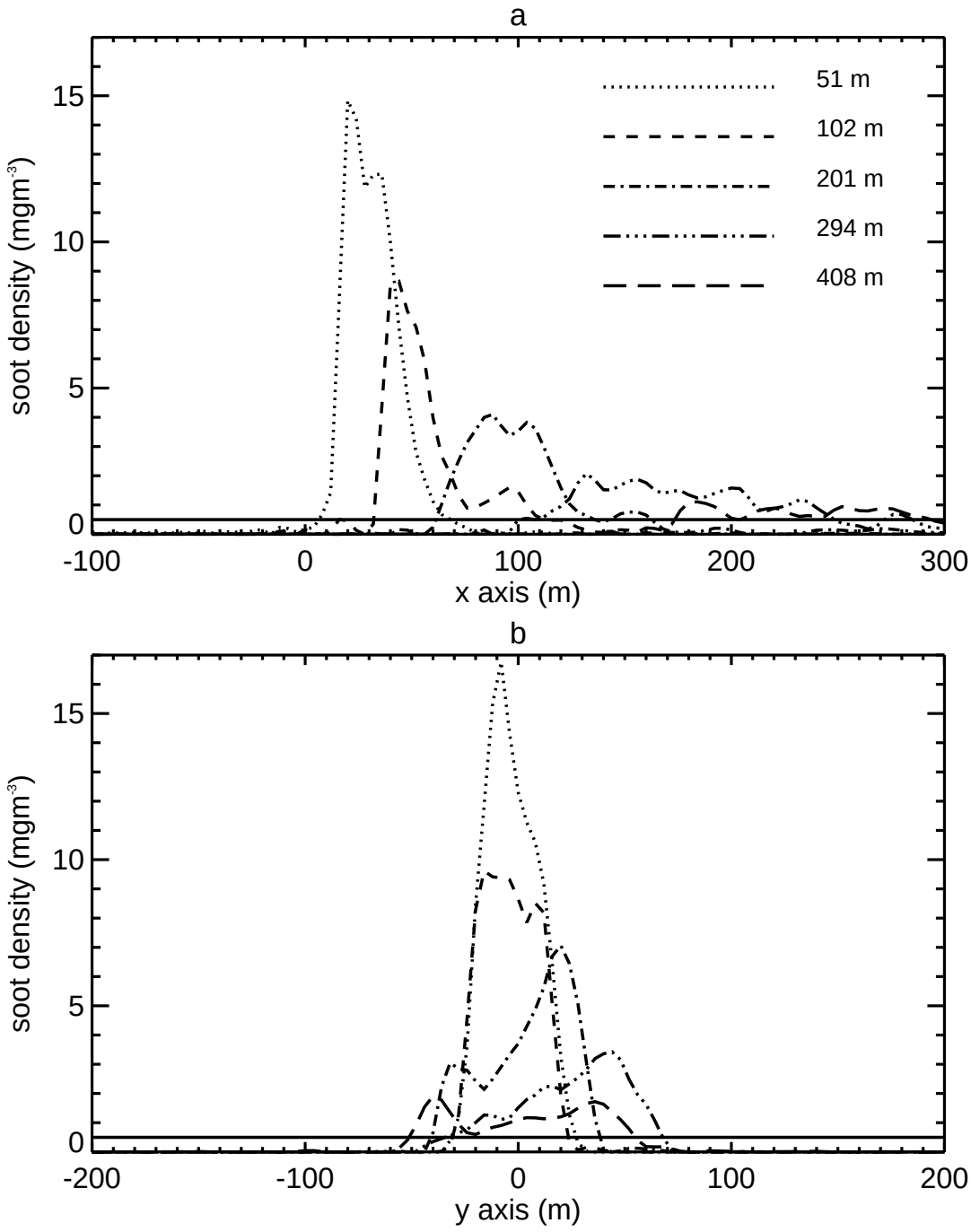

Figure 2: FDS radial profiles at different height levels and 600 s into the simulation of (a) soot density along the domain centerline in x direction and (b) through the point of maximum soot density in the y direction. Horizontal line denotes the soot density of 0.5 mg m^{-3} selected to delineate the plume edge.

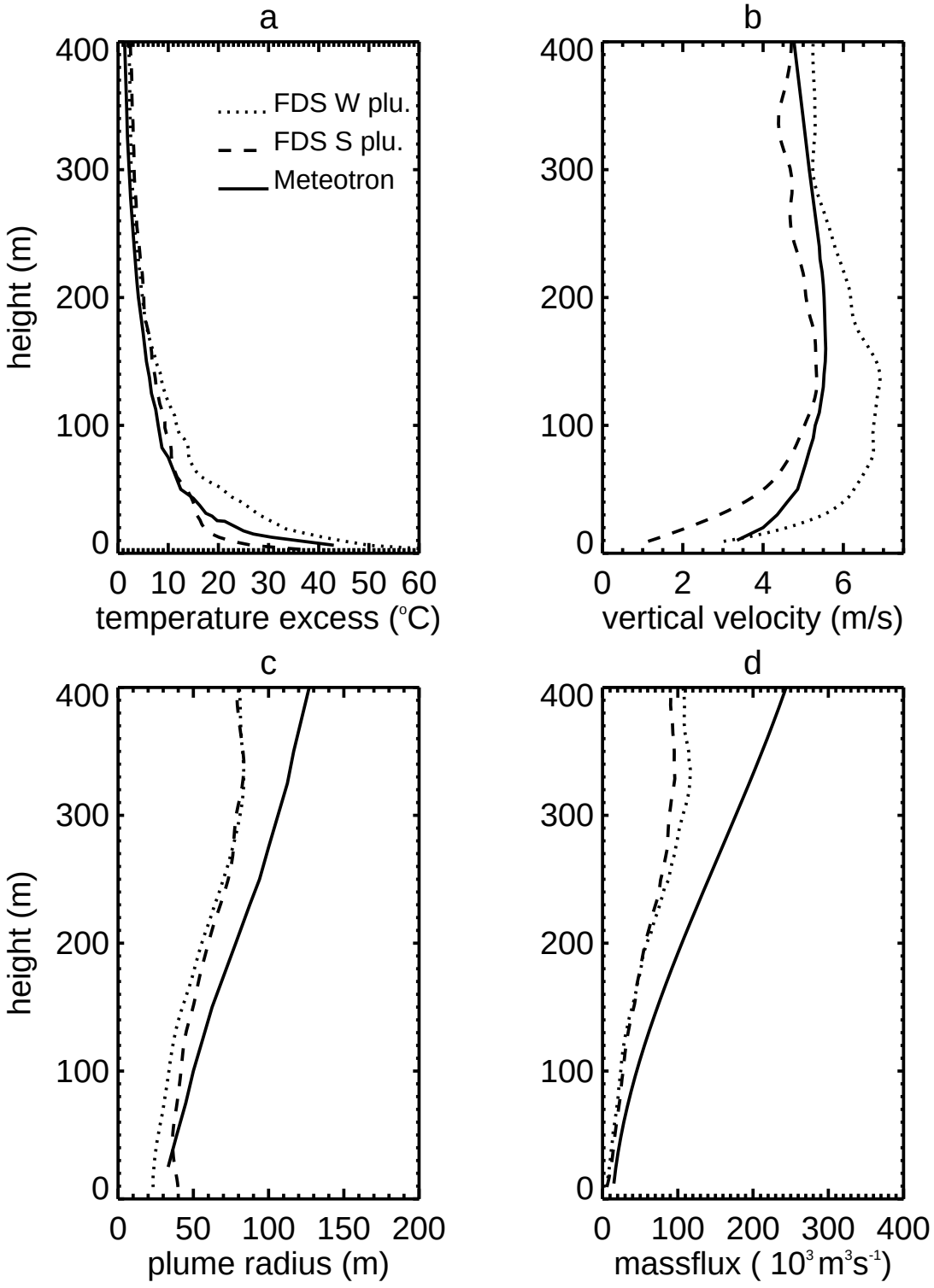

Figure 3: Vertical profiles of plume–averaged properties in the Meteotron experiment (solid line), and FDS simulation determined by W (dotted line) and soot (dashed line) criteria.

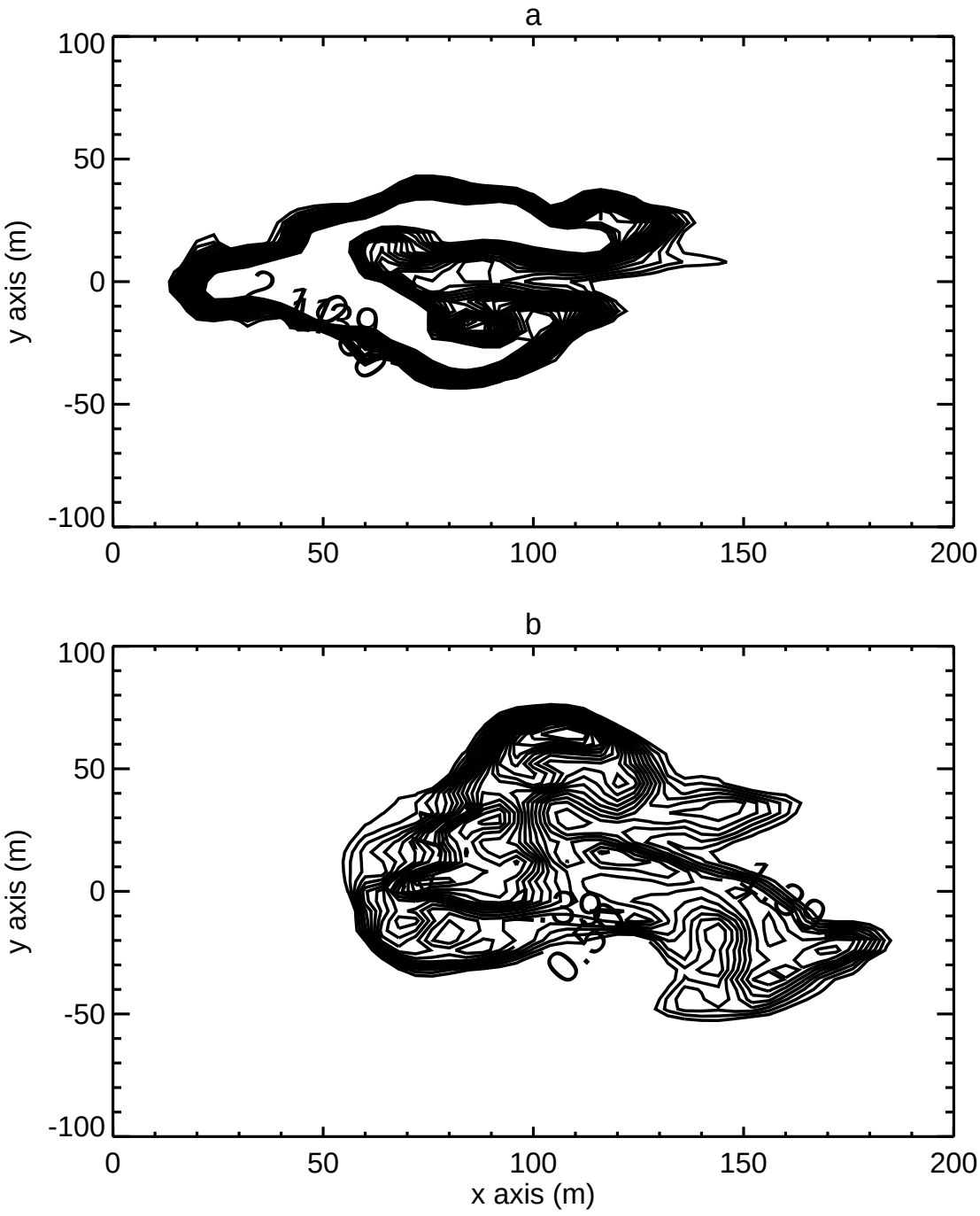

Figure 4: Soot density contours on a x-y cross-section of the plume at (a) 103 m AGL and (b) 201 m AGL at 680 s in FDS simulation.

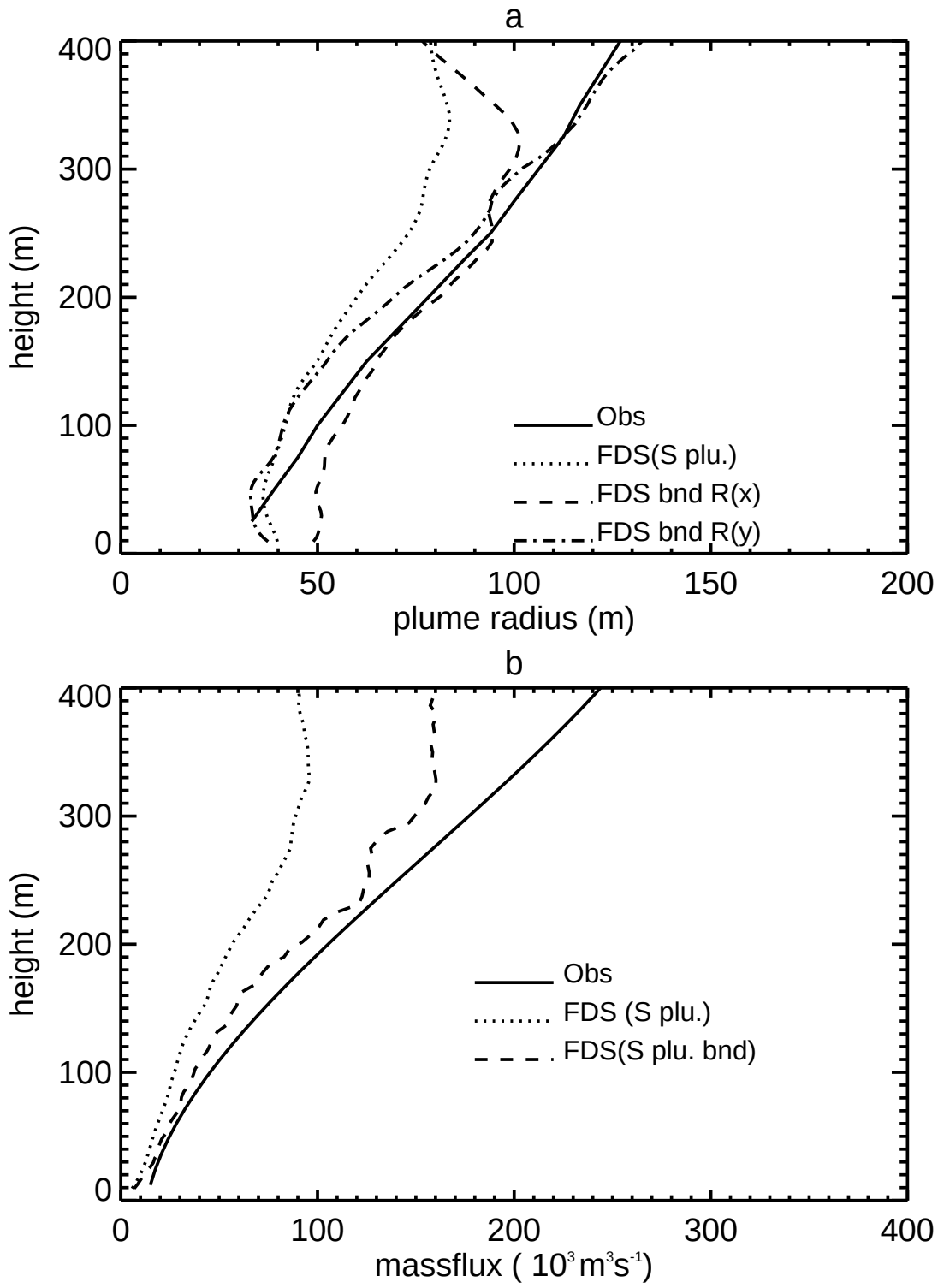

Figure 5: Vertical profiles of (a) Meteotron R (solid line), FDS soot–plume R (dotted line), FDS $R(x)$ plume radius (dashed line), and FDS $R(y)$ plume radius (dashed–dotted line). Vertical profiles of (b) Meteotron mass flux (solid line), FDS soot–plume mass flux based on R (dotted line), and FDS soot–plume mass flux based on $R(x)$ and $R(y)$ radii (dashed line).

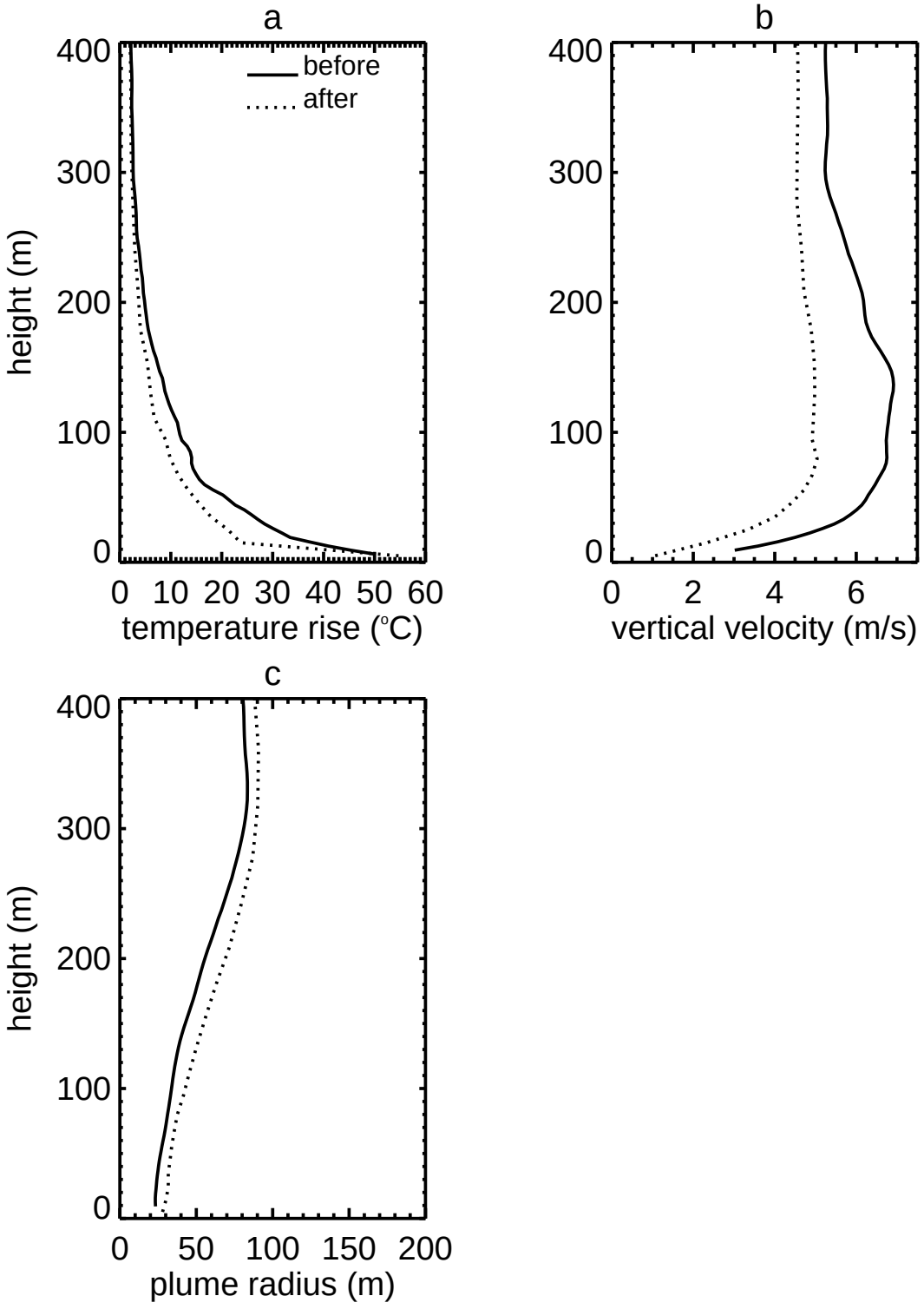

Figure 6: Vertical profiles of W–plume averaged properties in the FDS simulation before (solid line) and after (dotted line) averaging for comparisons between the Clark coupled model simulations and the FDS simulation.

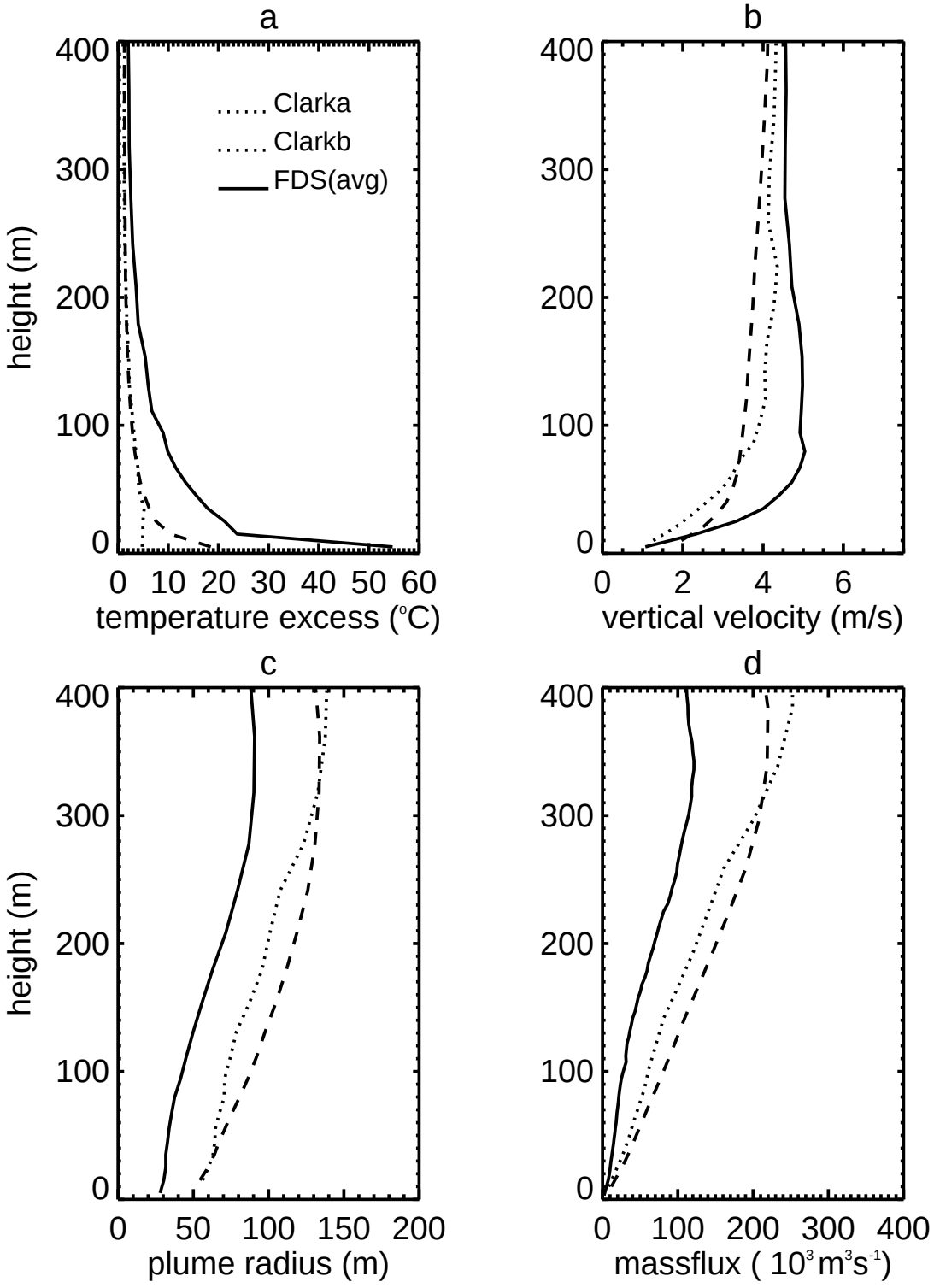

Figure 7: Vertical profiles of the FDS (solid line), *Clarka* (dotted line), and *Clarkb* (dashed line) W−plume averaged temperature excess, vertical velocity, plume radius, and plume mass flux.

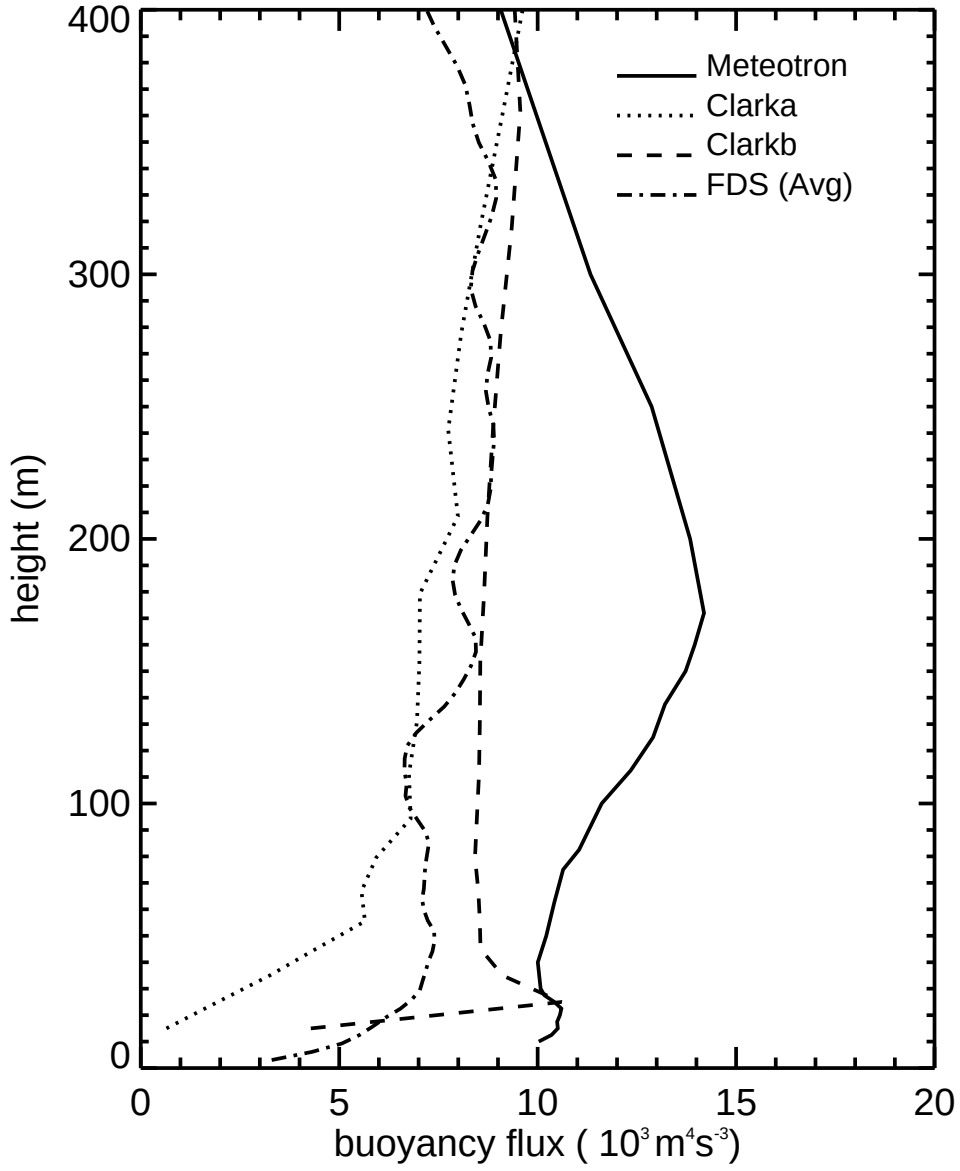

Figure 8: Vertical profiles of the Meteotron experiment (solid line), *Clarka* (dotted line), *Clarkb* (dashed line), and FDS (dotted–dashed line) W–plume averaged convective buoyancy fluxes based on Equation 3.

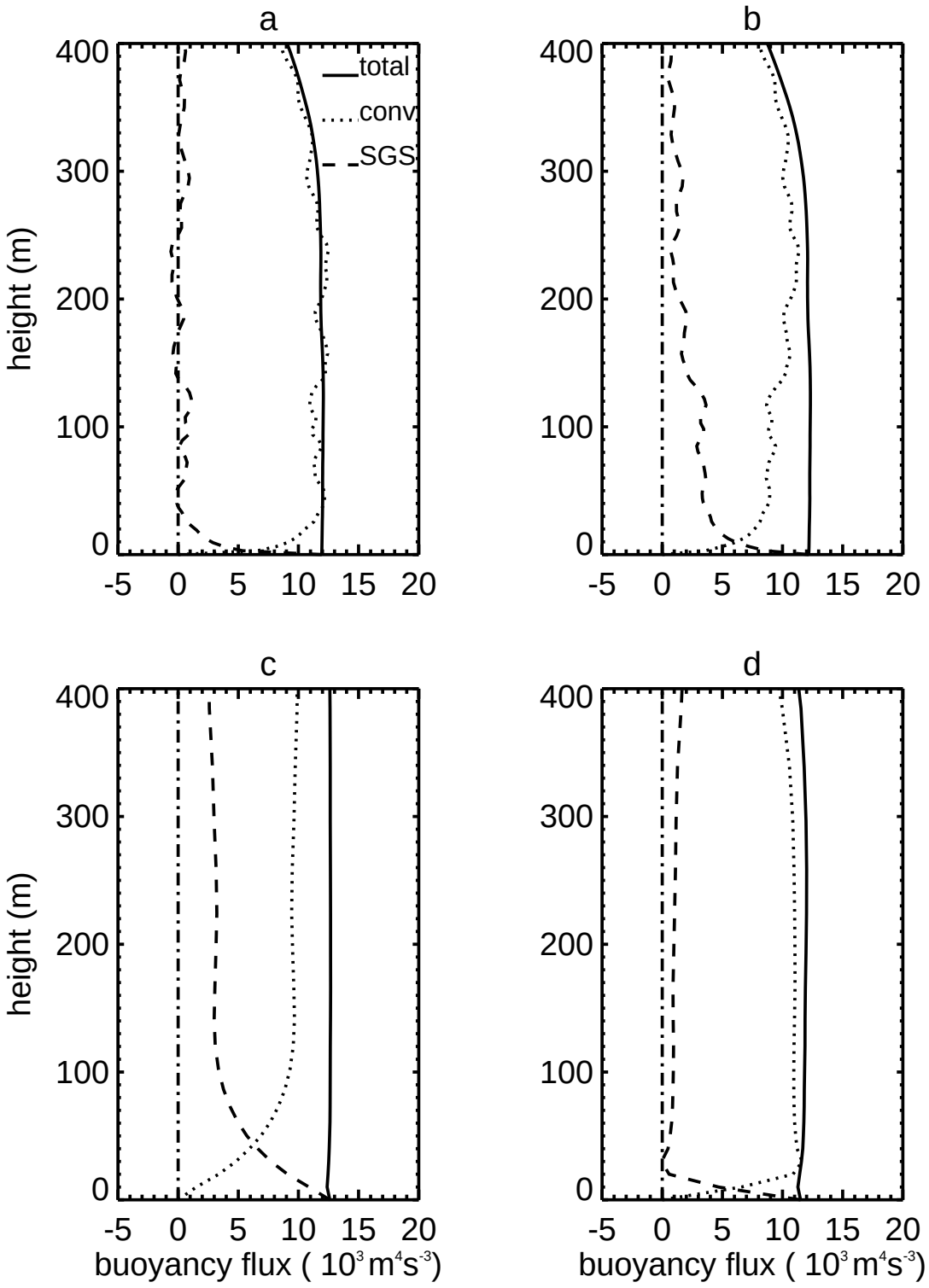

Figure 9: Vertical profiles of the total buoyancy flux (solid line), convective buoyancy flux (dotted line), and flux by SGS motion, radiation and combustion (dashed line) in the FDS simulation (a) before and (b) after grid–area averaging and in (c) *Clarka* and (d) *Clarkb*.